Development of open-source software $\mathcal{H}\Phi$

Mitsuaki Kawamura[a], Takahiro Misawa[a], Youhei Yamaji[b,c,d], Kazuyoshi Yoshimi[a]

[a]*Institute for Solid State Physics, University of Tokyo*
Kashiwa-no-ha, Kashiwa, Chiba 277-8581
[b]*Quantum-Phase Electronics Center (QPEC), The University of Tokyo*
Bunkyo-ku, Tokyo, 113-8656, Japan
[c]*Department of Applied Physics, The University of Tokyo*
Bunkyo-ku, Tokyo, 113-8656, Japan
[d]*JST, PRESTO*
Bunkyo-ku, Tokyo, 113-8656, Japan

Abstract

We overview "Project for advancement of software usability in materials science" (PASMS) managed by the center of the supercomputer at Institute for Solid State Physics (ISSP) in this activity report. In PASMS, we have supported the developments of the software packages that will be useful in a wide range of the condensed matter physics. In a part of the project, we have newly developed an open-source software package for the exact diagonalization $\mathcal{H}\Phi$. In this report, we focus on $\mathcal{H}\Phi$ and explain the basic properties including the user interfaces, the implemented modern algorithms, and the parallelization efficiency. We also show the applications of $\mathcal{H}\Phi$ to the frustrated Hubbard model and the Kitaev systems where the quantum spin liquids are expected to appear. The easy-to-use interface of $\mathcal{H}\Phi$ helps us to investigate these systems promptly by calculating the finite-temperature properties, low-energy excited state and the excitation spectrum of the quantum spin liquids. These applications show that $\mathcal{H}\Phi$ is a useful software package and has large spillover effects on the studies of condensed matter physics.

1 Introduction

From the 2015 fiscal year, the supercomputer center at ISSP has started PASMS [1]. In

Fiscal year	Software	Main proposer
2015	$\mathcal{H}\Phi$[3]	Youhei Yamaji
2015	OpenMX[4]	Taisuke Ozaki
2016	mVMC[5]	Takahiro Misawa
2016	$K\omega$[6]	Takeo Hoshi
2017	$\mathcal{H}\Phi$[3]	Youhei Yamaji
2017	DCore[7]	Hiroshi Shinaoka

Table 1: List of software packages developed in "Project for advancement of software usability in materials science".

PASMS, we have developed new software packages, implemented new functions to existing software, and supported for releasing software packages. As shown in Table 1, in one fiscal year, two software packages were supported by this project. These developed software packages are released as open-source software packages and thus can be utilized by a wide range of scientists working in materials science including the non-experts of the computational materials science such as the experimentalists. Furthermore, users can easily use these software packages on the supercomputer at ISSP because they are pre-installed in the supercomputer at ISSP [2].

In this activity report, we focus on a program package $\mathcal{H}\Phi$ [3, 8] newly developed by

PASMS. The core of $\mathcal{H}\Phi$ is numerical exact diagonalization for quantum lattice Hamiltonians. Before explaining the details of $\mathcal{H}\Phi$, we briefly summarize our motivation and aim for developing a new exact diagonalization package in this project. We note that there are several numerical diagonalization packages such as TITPACK [9], KOBEPACK [10] and SPIN-PACK [11]. Although these pioneering software packages are useful for treating conventional models such as the Heisenberg model and have been widely used for several decades in the community of the condensed matter physics, they are not suitable for the architecture of the modern supercomputers. For example, the distributed memory parallelization, is not supported in TITPACK and KOBEPACK. Although SPINPACK supports such parallelization, it does not support the general interactions that often appear in low-energy effective Hamiltonians for real materials. Moreover, the above packages do not support the modern algorithms such as the thermal pure quantum (TPQ) state approach [12, 13, 14, 15] for finite-temperature calculations, shifted Krylov subspace method [16, 17] for calculating the dynamical Green functions, and the locally optimal block preconditioned conjugate gradient (LOBPCG) method [18] for obtaining the many low-energy excited states at one calculation. Our aim of developing $\mathcal{H}\Phi$ is to provide a user-friendly, general-purpose, and parallelized diagonalization package that includes the above modern algorithms for the condensed matter community.

Here, in chronological order, we summarize the main functions/methods implemented in $\mathcal{H}\Phi$. In the 2015 fiscal year, we first implemented Lanczos and full diagonalization algorithms for obtaining the ground states and finite temperature calculations based on thermal pure quantum state approach [15]. We also designed a simple and flexible user interfaces that enable users to handle general interactions and also calculate physical quantities,

such as internal energy, temperature dependence of specific heat, and charge/spin structure factors. In the 2016 fiscal year, the numericallibrary $K\omega$[6] was developed by collaborating with scientists in mathematical physics. This library provides large-scale parallel computing algorithms for sparse matrices based on the shifted Krylov subspace method. By using $K\omega$, we implemented the shifted bi-conjugate gradient (sBiCG) method [16, 17] in $\mathcal{H}\Phi$ to obtain the dynamical Green functions and the excitation spectrum. We also implemented the locally optimal block preconditioned conjugate gradient (LOBPCG) method [18]. By using the LOBPCG method, users can compute several low-energy eigenvalues and eigenvectors simultaneously in one calculation. Furthermore, in the 2017 fiscal year, the real-time evolution was implemented to investigate the nonequilibrium states of the quantum many-body systems.

In this report, we explain the basic properties of $\mathcal{H}\Phi$ and show several applications. The organization of this report is as follows: In Sec. 2, we detail the target models, numerical methods, and the calculation flow of $\mathcal{H}\Phi$. We also show benchmark results of the parallelization of $\mathcal{H}\Phi$ on SGI ICE XA (Sekirei) at ISSP. In Sec. 3, as the demonstration of numerical analyses of $\mathcal{H}\Phi$, we show the applications of $\mathcal{H}\Phi$ to the quantum spin liquids. In Sec. 4, we summarize this report.

2 Basic properties

2.1 Models

By using $\mathcal{H}\Phi$, users can treat the general Hamiltonians defined as

$$\hat{\mathcal{H}} = \hat{\mathcal{H}}_0 + \hat{\mathcal{H}}_{\mathrm{I}}, \tag{1}$$

$$\hat{\mathcal{H}}_0 = \sum_{ij} \sum_{\sigma_1,\sigma_2} t_{i\sigma_1 j\sigma_2} \hat{c}^{\dagger}_{i\sigma_1} \hat{c}_{j\sigma_2}, \tag{2}$$

$$\hat{\mathcal{H}}_{\mathrm{I}} = \sum_{i,j,k,l} \sum_{\sigma_1,\sigma_2,\sigma_3,\sigma_4} I_{i\sigma_1 j\sigma_2 k\sigma_3 l\sigma_4} \hat{c}^{\dagger}_{i\sigma_1} \hat{c}_{j\sigma_2} \hat{c}^{\dagger}_{k\sigma_3} \hat{c}_{l\sigma_4},$$
$$\tag{3}$$

where $\hat{c}_{i\sigma}^{\dagger}$ $(\hat{c}_{i\sigma})$ is the creation (the annihilation) operator of an electron at site-i with spin-σ, and $t_{ij\sigma_1\sigma_2}$ and $I_{ijkl\sigma_1\sigma_2\sigma_3\sigma_4}$ are the one-body potentials and two-body interactions, respectively. As an special case of the above general Hamiltonian, we can treat spin 1/2 localized spin systems and the Kondo systems, where the itinerant electrons couple with the spin 1/2 localized spins. $\mathcal{H}\Phi$ can also treat quantum spin systems with arbitrary spin whose amplitude s larger than 1/2, i.e, $S = 1, 3/2, 2, \ldots$ and mixed-spin systems.

2.2 Method

2.2.1 Eigenvectors by the Lanczos and the LOBPCG method

To obtain the eigenvalues and eigenvectors of the quantum lattice Hamiltonians, the Lanczos method [19] has been employed in the previous packages. In this method, we compute eigenvalues by diagonalizing the tri-diagonal matrix that is generated by multiplying the Hamiltonian to the initial vector. The Lanczos method, however, has two problems. One is that eigenvectors can not be obtained in a set of the Lanczos process. If we need eigenvectors, we must perform the same Lanczos process again. Moreover, generally, the obtained eigenvector is not accurate enough and we have to refine the obtained eigenvector with the inverse iteration method. The other problem is that the Lanczos method cannot compute the number of degeneracy in one calculation. To determine the degeneracy, it is necessary to perform the several Lanczos calculations for different initial vectors and orthogonalize the obtained eigenvectors. This redundancy is a main weak point in the Lanczos method.

To overcome this weak point, we employ LOBPCG method in $\mathcal{H}\Phi$ [18]. In this method, we obtain M eigenvectors from the subspace spanned by $3M$ vectors

$$\{ \, | \, \Phi_1^{(i)}\rangle, \, | \, \Phi_2^{(i)}\rangle, \cdots, \, | \, \Phi_M^{(i)}\rangle \, \}, \qquad (4)$$

$$\{ \, | \, r_j^{(i)}\rangle = \hat{\mathcal{H}} \, | \, \Phi_j^{(i)}\rangle - \varepsilon_j^{(i)} \, | \, \Phi_j^{(i)}\rangle \, \}, \qquad (5)$$

$$\{ \, | \, \Phi_1^{(i-1)}\rangle, \, | \, \Phi_2^{(i-1)}\rangle, \cdots, \, | \, \Phi_M^{(i-1)}\rangle \, \}, \qquad (6)$$

at each iteration, where $|\Phi_j^{(i)}\rangle$ is the jth eigenvector at the ith iteration and $\varepsilon_j^{(i)} = \langle\Phi_j^{(i)}|\hat{\mathcal{H}}|\Phi_j^{(i)}\rangle$. This method allows us to simultaneously obtain arbitrary number of excited states in one calculation. We will show an example of the calculation for the frustrated Hubbard model in Sec. 3.

2.2.2 Finite-temperature properties by the TPQ state

Recently, an efficient unbiased numerical method for calculating finite-temperature properties in quantum systems is proposed [15]. In this method, thermodynamic properties such as internal energy and the correlation functions are given as expectation values of *one* TPQ state for sufficiently large system sizes. This method enables us to calculate the finite-temperature properties *without* ensemble average and perform the unbiased finite-temperature calculations for a large system size to which full diagonalization method is almost inapplicable. We note that, the idea for calculating the finite-temperature properties without ensemble average were proposed in the pioneering works [12, 20, 21, 22]. In some of these papers, the finite-temperature observables were already calculated by replacing ensemble average with random sampling of wave functions.

We explain how to construct the TPQ state [15], which offers a simple way for finite-temperature calculations. Let $|\psi_0\rangle$ be a random initial vector. By operating $(l - \hat{\mathcal{H}}/N_{\mathrm{s}})^k$ (l is a constant, N_{s} represents the number of sites) to $|\psi_0\rangle$, we obtain the k-th TPQ states as

$$|\psi_k\rangle \equiv \frac{(l - \hat{\mathcal{H}}/N_{\mathrm{s}}) \, |\psi_{k-1}\rangle}{|(l - \hat{\mathcal{H}}/N_{\mathrm{s}}) \, |\psi_{k-1}\rangle \, |}. \qquad (7)$$

From $|\psi_k\rangle$, we estimate the corresponding inverse temperature β_k as

$$\beta_k \sim \frac{2k/N_s}{l - u_k}, \qquad u_k = \langle\psi_k|\hat{\mathcal{H}}|\psi_k\rangle/N_s, \quad (8)$$

where u_k is the internal energy. Arbitrary local physical properties at β_k are also estimated as

$$\langle\hat{A}\rangle_{\beta_k} = \langle\psi_k|\hat{A}|\psi_k\rangle/N_s. \quad (9)$$

In a finite-size system, a finite statistical fluctuation is caused by the choice of the initial random vector. To estimate the average value and the error of the physical properties, we perform some independent calculations by changing $|\psi_0\rangle$. Usually, we regard the standard deviations of the physical properties as the error bars.

2.2.3 Dynamical structure factors by the shifted Krylov method

In $\mathcal{H}\Phi$, users can calculate the dynamical correlation function defined as

$$G_{\alpha\beta}(\omega) = \langle\Phi_0|\hat{A}_\alpha^\dagger(\omega - \hat{H})^{-1}\hat{A}_\beta|\Phi_0\rangle, \quad (10)$$

where $|\Phi_0\rangle$ is the initial wavefunction, and $\hat{A}_\alpha$ and $\hat{A}_\beta$ are the excited operators. When $\alpha = \beta$, this quantity can be computed by the continued fraction algorithm and the elements of the tri-diagonal matrix obtained in the Lanczos method [19]. However, this conventional method is not applicable to the case that $\alpha \neq \beta$.

In $\mathcal{H}\Phi$, we employ the shifted Krylov method [17] which can compute both diagonal and off-diagonal dynamical correlation functions as follows:

$$|b_\beta\rangle = \hat{A}_\beta|\Phi_0\rangle \quad (11)$$

$$(\omega - \hat{\mathcal{H}})|x_\beta(\omega)\rangle = |b_\beta\rangle \quad (12)$$

$$G_{\alpha\beta}(\omega) = \langle b_\alpha|x_\beta(\omega)\rangle. \quad (13)$$

The series of the linear equations (12) can be solved simultaneously by using sBiCG method [16]. The sBiCG method is based on
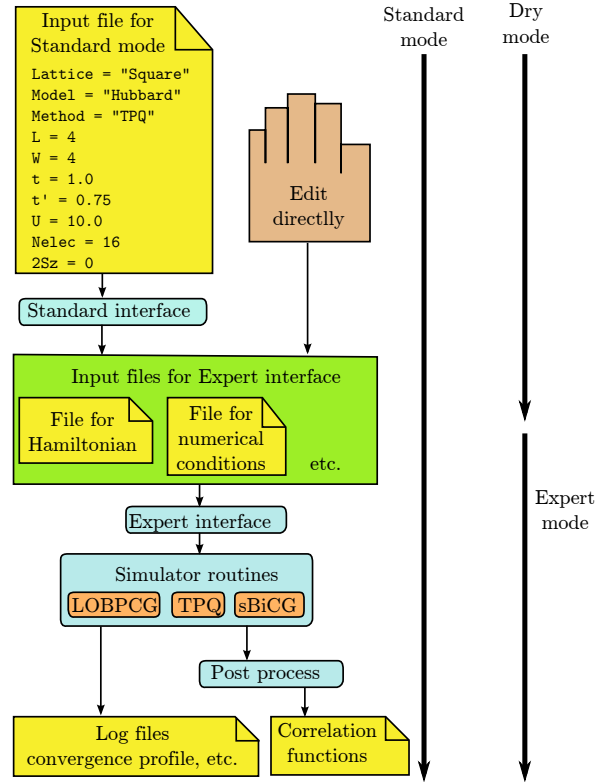

Figure 1: Calculation flow of $\mathcal{H}\Phi$.

the shift invariance of the Krylov subspace, which is defined as

$$\mathcal{K}_n(\omega) = \{|b_\beta\rangle, (\omega - \hat{\mathcal{H}})|b_\beta\rangle, \ldots, (\omega - \hat{\mathcal{H}})^{n-1}|b_\beta\rangle\}. \quad (14)$$

Shift invariance means that spanned subspace by $\mathcal{K}_n(\omega)$ do not depend on ω, i.e., span$\{\mathcal{K}_n(\omega)\}$ = span$\{\mathcal{K}_n(\omega')\}$. Due to the shift invariance, if we once obtain $G_{\alpha\beta}(\omega)$ for given ω, we can obtain the arbitrary $G_{\alpha\beta}(\omega')$ from $G_{\alpha\beta}(\omega)$. This means that the numerical cost of this method does not depend on the number of frequencies. This efficient method is implemented in $\mathcal{H}\Phi$ by using $K\omega$ library [6], which is also developed in this project.

2.3 Calculation flow and user interfaces

A typical calculation flow in $\mathcal{H}\Phi$ is shown in Fig. 1. If the target system is supported by Standard mode, only one input file is necessary

for a calculation. For example, in the left top panel in Fig. 1, we show an example of input file for the TPQ calculation (`Method="TPQ"`) in the Hubbard model (`Model="Hubbard"`) on the square lattice (`Lattice="Square"`). In the input file, we set the nearest-neighbor hopping as `t=1`, the second nearest-neighbor hopping as `t'=0.75`, on-site Coulomb interaction as `U=10`, the width of cell as `W=4`, the length of cell as `L=4` (16 sites), number of electrons as `Nelec=16`, and the double of the total z component of spin as `2Sz=0`. From this file, $\mathcal{H}\Phi$ generates input files for Expert mode, which specify the Hamiltonian and the details of the numerical conditions. Then, $\mathcal{H}\Phi$ performs the TPQ calculations by reading these automatically generated input files. After the calculation, we can obtain the temperature dependence of the physical properties and the elapsed time in the generated log files. We can also plot the correlation function in the reciprocal space by using the utility tool to perform the Fourier transformation (Fourier tool).

If users want to compute more complicated system that is not supported in Standard mode, users should prepare the input files in Expert mode. Using Dry model is a convenient way for generating input files in Expert mode. By using the Dry mode, only the input files in Expert mode are generated without calculations. By editing the generated input files for the standard models, users can treat more general models in Expert mode.

2.4 Performance of parallelization

Here, we show benchmark result of the parallelization in $\mathcal{H}\Phi$. To examine the efficiency of the parallelization of $\mathcal{H}\Phi$, we carry out TPQ simulations for half-filled 18-site Hubbard model with $S_z = 0$ on the square lattice shown in the inset of Fig. 2 with varying numbers of threads and processes. In this system, the dimension of the Hilbert space is given by $(_{18}C_9)^2 = 2,363,904,400$, where $_aC_b$ represents the binomial coefficient.
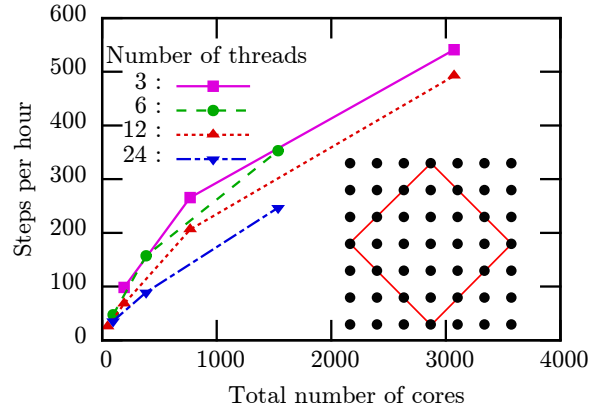

Figure 2: Speedup of TPQ calculations with hybrid parallelization by using up to 3,072 cores on Sekirei [8]. The squares, circles, upward triangles, and downward triangles represent the results with 3 threads, 6 threads, 12 threads, and 24 threads, respectively. The inset shows the shape of the 18-site cluster used in the benchmark calculations.

In Fig. 2, we show TPQ steps per hour up to 3,072 cores at SGI ICE XA (Sekirei) at ISSP. We can see significant acceleration caused by the increase of CPU cores. This acceleration is almost linear up to 192 cores, and is weakened as we further increase the number of cores. This weakening of the acceleration may come from the load imbalance in the S^z conserved simulation. This imbalance is expected to be solved by using randomly distributed memory parallelization [23].

3 Result

In this section, we show applications of $\mathcal{H}\Phi$ to the quantum spin liquids in the frustrated Hubbard model and the Kitaev systems.

3.1 Application to the frustrated Hubbard model

The Hubbard model with the next-nearest-neighbor (nnn) hopping t' on the square lattice [see, Fig. 3(a)] is a prototypical system for
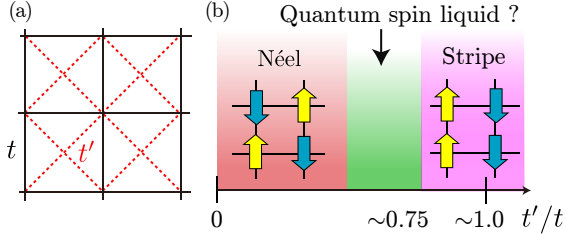
Figure 3: (a) Schematic picture for frustrated Hubbard model. (b) Schematic phase diagram for the frustrated Hubbard model in the strong coupling region.

studying the quantum spin liquids induced by the geometrical frustrations. In the following, we focus on half filling, i.e., the filling is given by $n = N_s^{-1} \sum_{i\sigma} \langle c_{i\sigma}^\dagger c_{i\sigma} \rangle = 1$ ($N_s = L \times L$ is the system size). To reduce the numerical cost, we only consider the total $S_{total}^z = 0$ space, i.e., $S_{total}^z = \sum_i S_i^z = 0$. We employ a $N_s = 16 = 4 \times 4$ cluster with the periodic-periodic boundary condition and a $N_s = 18 = 3\sqrt{2} \times 3\sqrt{2}$ cluster with antiperiodic-periodic boundary condition.

In the strong coupling region ($U/t >> 1$, where U is the on-site Coulomb integral), the nearest-neighbor (next-nearest-neighbor) superexchange interactions J_1 (J_2) are given by $J_1 = 4t^2/U$ ($J_2 = 4t'^2/U$). From this, in the strong coupling region, simple Néel magnetic order is expected to appear around $t' = 0$ and the stripe magnetic order is expected to appear around $t'/t = 1$ as shown in Fig. 3(b). In fact, highly-accurate numerical calculations at zero temperature have shown that the expected magnetic orders appear for both the t-t' Hubbard model [24, 25, 26] and the J_1-J_2 Heisenberg model [27, 28, 29, 30].

In the intermediate region where J_1 and J_2 competes, i.e., $J_2/J_1 \sim 0.5$ [27, 28, 29, 30] or $t'/t \sim 0.75$ [24, 25, 26], it has been proposed that the quantum spin liquid appears. In spite of the huge number of the ground-state calculations, finite-temperature properties have not been systematically studied so far due to the lack of the efficient numerical method. Because the errors of TPQ method are determined by the entropy [15, 31], the TPQ method is useful for studying the finite-temperature properties of the quantum spin liquids, where the entropy is expected to remain large. Although the applicable system sizes of the TPQ method are limited to small system sizes such as $N_s = 16(4 \times 4)$ for the frustrated Hubbard model, we find the signature of the quantum spin liquid at the moderately high-temperature region where the finite-system size effects are small.

In Fig. 4(a), we show temperature dependence of the specific heat, which is defined as

$$C/N_s = (\langle \hat{\mathcal{H}}^2 \rangle - \langle \hat{\mathcal{H}} \rangle^2)/(N_s T^2). \qquad (15)$$

The high-temperature peaks ($T/t \sim 2$) in the specific heat are governed by the energy scale of U and do not depend on t'. In contrast to this, the low-temperature peaks are governed by the super exchange interactions and largely depend on t'. When the ground states are magnetically ordered state, i.e., Néel state ($t'/t = 0.5$) or stripe state ($t'/t = 1.0$), obvious low-temperature peaks exist while peak height is reduced for $t'/t = 0.75$ where the quantum spin liquid is expected to appear. This indicates that the entropy remains large around $t'/t = 0.75$.

We now examine the temperature dependence of the entropy, which is defined as

$$S(T)/N_s = c \ln 2 - \frac{1}{N_s} \int_\infty^T \frac{C}{T dT},$$

$$S_{norm} = \frac{1}{c \ln 2} \frac{S(T)}{N_s}. \qquad (16)$$

Because we restrict the Hilbert space with the fixed particle number and $S_z = 0$, the normalization factors c appears in the definition of the entropy. The normalization factor is given by $c \sim 1.706$ for 16 sites. As shown in Fig. 4(b), we find that the entropy remains large at $t'/t = 0.75$ compared to the other t'.

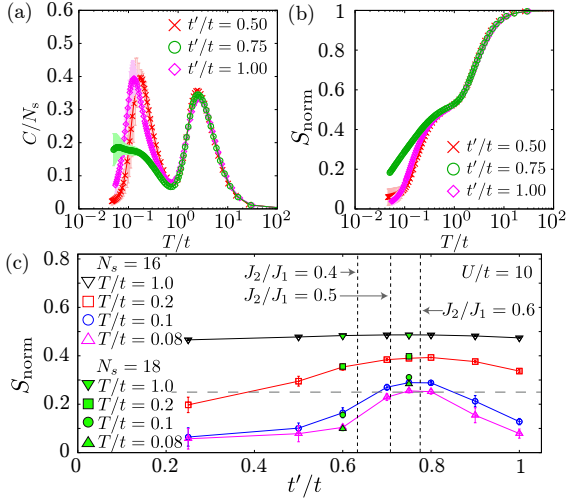Furthermore, we plot the t' dependence of the finite-temperature entropy in Fig. 4(c).

Figure 4: (a) Temperature dependence of the specific heat for $U/t = 10$. (b) Temperature dependence of the entropy for $U/t = 10$. (c) Frustration (t'/t) dependence of the entropy at fixed temperatures for $N_{\rm s} = 16$ and $N_{\rm s} = 18$. Around $t'/t \sim 0.75$, the entropy remains large at moderately high-temperature and shows a peak structure. The large remaining entropy is the signature of the quantum spin liquid.

As a result, we find that the entropy has peak structure, in the intermediate region ($t'/t \sim 0.75$) even at moderately high-temperature ($T/t \sim 0.1$). By calculating $N_{\rm s} = 18$ site cluster, we confirm that the finite-size effects are small at this temperature range. This large remaining entropy at moderately high-temperature ($T/t \sim 0.1$) offers an useful criterion whether the target systems have a chance to be quantum spin liquid or not.

By using LOBPCG method implemented in $\mathcal{H}\Phi$, it is possible to obtain the several low-energy exited states. In Fig. 5, we show an example of the LOBPCG calculations for the frustrated Hubbard model shown in the previous section. In the calculations, we obtain 16 lowest eigenvalues and eigenvectors simultaneously. We can see the degeneracy of the eigenvalues is large for $t'/t = 0.75$ and it is consistent with the large remaining entropy at finite temperatures.
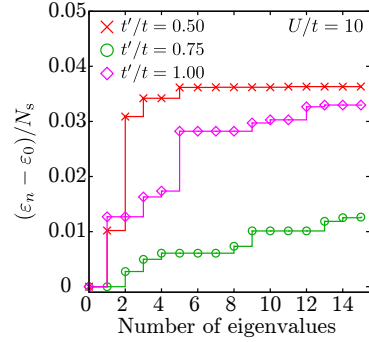

Figure 5: Eigenvalues obtained by the LOBPCG method for the frustrated Hubbard model. The n-th eigenvalues are denoted by ε_n (ε_0 represents the ground state energy).

3.2 Application to Kitaev systems

In this section, we show dynamical spin structure factors of the Kitaev model [32] and *ab initio* effective Hamiltonian of the related iridium oxide Na_2IrO_3 [33] simulated by the sBiCG method. These systems show complicated spin excitation continua in contrast to spin wave spectra in typical magnets such as the Heisenberg model on a square lattice. In addition, the Kitaev model and the *ab initio* effective Hamiltonian show remarkably different convergences of the sBiCG method, which are quantified by the norm of the residual vectors in each sBiCG step.

The Kitaev model on the honeycomb structure is an exactly solvable quantum spin $S = 1/2$ system defined as

$$\hat{\mathcal{H}}_{\rm K} = \sum_{\langle i,j \rangle_x} K_x \hat{S}_i^x \hat{S}_j^x + \sum_{\langle i,j \rangle_y} K_y \hat{S}_i^y \hat{S}_j^y + \sum_{\langle i,j \rangle_z} K_z \hat{S}_i^z \hat{S}_j^z, \tag{17}$$

where $\langle i,j \rangle_\gamma$ ($\gamma = x, y, z$) represents a pair of the nearest neighbor sites along γ-bond illustrated in Fig. 6(a), and K_γ is a bond-direction dependent Ising coupling. The Kitaev model has attracted considerable attention due to its spin liquid ground state and the emergent fractionalization of spin degrees of freedom [32]. Due to the fractionalization, the dynamical

spin structure factor of the Kitaev model shows excitation continuum.

Although the Kitaev model seems to be an artificial model and to be difficult to realize in real materials, Jackeli and Khaliullin proposed that low-energy physics of an iridium oxide Na_2IrO_3 is described by the Kitaev model [33]. Even though the experimental observations reveal the magnetically ordered ground state of Na_2IrO_3 [34], theoretical researchers tried to write down the effective Hamiltonian of the iridium oxides to figure out how to realize the *Kitaev materials.* One of the authors and his colleagues derived the *ab initio* Hamiltonian of Na_2IrO_3 [35] and found that the dominant energy scale of the effective Hamiltonian is indeed given by the Kitaev's bond-dependent Ising couplings $K_x = K_y = -23.9$ meV and $K_z = -30.7$ meV while there are other small but finite couplings even in the nearest neighbor couplings. In addition, there are the second and third neighbor couplings (see the reference [35] for the details). Although the effective Hamiltonian shows the magnetically ordered ground state consistent with the experiments, it is expected that the signature of the fractionalization can be seen in the spin excitation.

To see the signature of the fractionalization we calculate the spin excitation by using the sBiCG method. The controlled convergence of the sBiCG enables us to examine the detailed spin excitation continuum obtained by calculating dynamical spin structure factor,

$$S(\vec{Q}, \omega) = -\frac{1}{\pi} \text{Im} \sum_{\gamma=x,y,z} \langle \Phi_0| \hat{S}^\gamma(\vec{Q})^\dagger$$
$$\times (\omega + i\delta + \varepsilon_0 - \hat{\mathcal{H}})^{-1} \hat{S}^\gamma(\vec{Q}) |\Phi_0\rangle, \quad (18)$$

where the broadening factor is chosen as $\delta = |K_z|/100$ and $\hat{S}^\gamma(\vec{Q}) = N_s^{-1/2} \sum_i \hat{S}_i^\gamma e^{i\vec{Q} \cdot \vec{r}_i}$. We choose $\vec{Q}$ along symmetry lines in the Brillouin zone shown in Fig. 6(b). First, the convergence of the sBiCG steps for excitation spectra is examined for the Kitaev model $\hat{\mathcal{H}}_K$ and the *ab initio* Hamiltonian $\hat{\mathcal{H}}_K + \hat{\mathcal{H}}'$, where $\hat{\mathcal{H}}'$ includes complicated interactions other than the
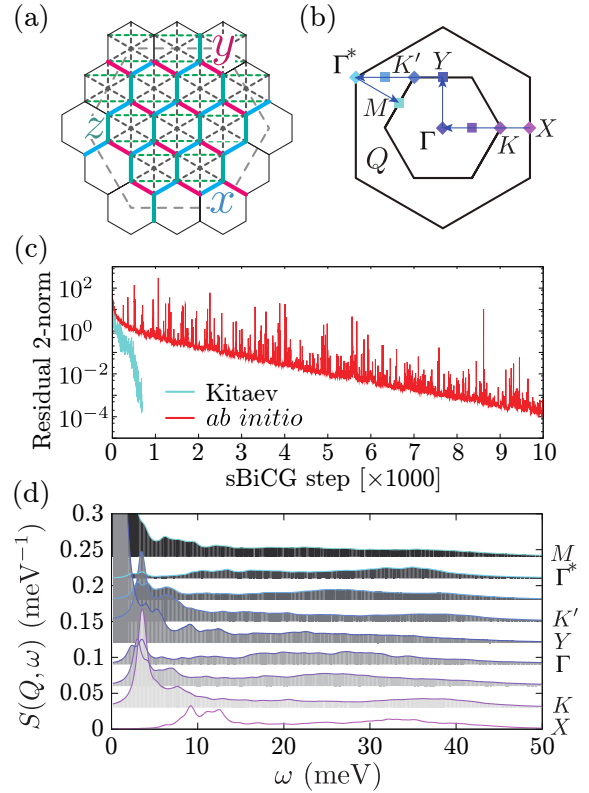

Figure 6: (a) 24 site cluster of the Kitaev and *ab initio* Hamiltonian. (b) Brillouin zone of honeycomb structure and symmetric momenta. (c) sBiCG step dependence of 2-norm of residual vectors for the Kitaev and *ab initio* Hamiltonian. (d) Dynamical spin structure factors of the *ab initio* Hamiltonian calculated by using sBiCG method.

Kitaev interactions. As shown in Fig. 6(c), the sBiCG step dependence of the 2-norm of the residual vector depends on the Hamiltonians. While the residual vector of the Kitaev model shows faster decay within thousand sBiCG steps, the residual vector of the *ab initio* Hamiltonian shows one order of magnitude slower convergence. The slower convergence may suggest larger density of states in the excitation spectrum. The significant dependence of the convergence on the Hamiltonians hampers *a priori* choice of number of the sBiCG steps. However, the sBiCG method enables us to control the convergence by examining the

sBiCG step dependence of the residual vector.

Figure 6(d) shows detailed continuum in the spin excitation spectrum of Na_2IrO_3 obtained by sBiCG. The proximity of the Kitaev's spin liquid phase is evident in the excitation continuum up to 40 meV.

4 Summary

In this report, we first explained "Project for advancement of software usability in materials science"(PASMS) in Sec. 1. As one of the achievements in this project, we focused on an open-source software package for the exact diagonalization, $\mathcal{H}\Phi$ and explained the target models, algorithms, and usage of $\mathcal{H}\Phi$ in Sec. 2. In this section, we also showed that $\mathcal{H}\Phi$ has good parallelization efficiency on Sekirei at ISSP by seeing the drastically acceleration with the increase of CPU cores. In Sec. 3, we showed applications of $\mathcal{H}\Phi$ to the frustrated Hubbard models and the Kitaev models, both of which are candidates of quantum spin liquids. For the frustrated Hubbard model, we studied finite-temperature properties by the TPQ method, and found that an entropy at moderately high-temperature remains large around the quantum spin liquids. For the Kitaev systems, we studied dynamical spin structure factors by using the sBiCG method considering a simple Kitaev model and a low-energy effective Hamiltonian of Na_2IrO_3 obtained by downfolding using outputs of the first-principles calculation. By careful analysis, we concluded that the remnant of the continuous spin excitations observed in the Kitaev model still remains in a realistic model of Na_2IrO_3.

As demonstrated in these two applications, $\mathcal{H}\Phi$ provides a powerful tool for analyzing exotic phases in quantum many-body systems. To further improve the functionality of $\mathcal{H}\Phi$ and make the closer comparisons possible, we will implement algorithms for simulating finite-temperature spectra [36] and will combine data science approaches [37] in the near future. We believe that $\mathcal{H}\Phi$ is useful for a wide range of the scientists in the filed of condensed matter physics and will accelerate developing material designs by promoting close collaboration between theories and experiments.

Acknowledgment

References

[1] http://www.issp.u-tokyo.ac.jp/supercom/softwaredev

[2] http://www.issp.u-tokyo.ac.jp/supercom/visitor/applications

[3] https://github.com/issp-center-dev/HPhi

[4] http://www.openmx-square.org

[5] https://github.com/issp-center-dev/mVMC

[6] https://github.com/issp-center-dev/Komega/releases

[7] https://github.com/
issp-center-dev/DCore

[8] M. Kawamura, K. Yoshimi, T. Misawa, Y. Yamaji, S. Todo, N. Kawashima, Comp. Phys. Commun. **217**, 180 (2017).

[9] http://www.stat.phys.titech.ac.jp/
~nishimori/titpack2_new/index-e.
html

[10] http://quattro.phys.sci.kobe-u.ac.
jp/Kobe_Pack/Kobe_Pack.html

[11] http://www-e.uni-magdeburg.de/
jschulen/spin/

[12] M. Imada, M. Takahashi, J. Phys. Soc. Jpn. **55**, 3354 (1986).

[13] J. Jaklič, P. Prelovšek, Phys. Rev. B **49**, 5065 (1994).

[14] A. Hams, H. De Raedt, Phys. Rev. E **62**, 4365 (2000).

[15] S. Sugiura, A. Shimizu, Phys. Rev. Lett. **108**, 240401 (2012).

[16] A. Frommer, Computing **70**, 87 (2003).

[17] S. Yamamoto, T. Sogabe, T. Hoshi, S.-L. Zhang, T. Fujiwara, J. Phys. Soc. Jpn. **77**, 114713 (2008).

[18] A. V. Knyazev, SIAM J. Sci. Comput. **23**, 517 (2001).

[19] E. Dagotto, Rev. Mod. Phys. **66**, 763 (1994).

[20] J. Jaklič, P. Prelovšek, Phys. Rev. B **49**, 5065 (1994).

[21] A. Hams, H. De Raedt, Phys. Rev. E **62**, 4365 (2000).

[22] S. Lloyd, arXiv:1307.0378.

[23] A. Wietek, A. M. Lauchli, arXiv:1804.05028.

[24] T. Kashima, M. Imada, J. Phys. Soc. Jpn. **70**, 3052 (2001).

[25] T. Mizusaki, M. Imada, Phys. Rev. B **74**, 014421 (2006).

[26] L. F. Tocchio, F. Becca, A. Parola, S. Sorella, Phys. Rev. B **78**, 041101 (2008).

[27] H.-C. Jiang, H. Yao, L. Balents, Phys. Rev. B **86**, 024424 (2012).

[28] W.-J. Hu, F. Becca, A. Parola, S. Sorella, Phys. Rev. B **88**, 060402 (2013).

[29] S.-S. Gong, W. Zhu, D. N. Sheng, O. I. Motrunich, M. P. A. Fisher, Phys. Rev. Lett. **113**, 027201 (2014).

[30] S. Morita, R. Kaneko, M. Imada, J. Phys. Soc. Jpn. **84**, 024720 (2015).

[31] S. Sugiura, A. Shimizu, Phys. Rev. Lett. **111**, 010401 (2013).

[32] A. Kitaev, Ann. Phys. **321**, 2 (2006).

[33] G. Jackeli, G. Khaliullin, Phys. Rev. Lett. **102**, 017205 (2009).

[34] F. Ye, S. Chi, H. Cao, B. C. Chakoumakos, J. A. Fernandez-Baca, R. Custelcean, T. F. Qi, O. B. Korneta, G. Cao, Phys. Rev. B **85**, 180403 (2012).

[35] Y. Yamaji, Y. Nomura, M. Kurita, R. Arita, M. Imada, Phys. Rev. Lett. **113**, 107201 (2014).

[36] Y. Yamaji, T. Suzuki, M. Kawamura, arXiv:1802.02854.

[37] R. Tamura, K. Hukushima, Phys. Rev. B **95**, 064407 (2017).